Complete Structure of *anti*-1,1,2,2-Tetrafluoroethane by High-Resolution Infrared Spectroscopy

Norman C. Craig,* Catherine M. Oertel, and David C. Oertel

Department of Chemistry, Oberlin College, Oberlin, Ohio 44074

Michael Lock

Physikalisch-Chemisches Institut der Justus-Liebig-Universität, Heinrich-Buff-Ring 58, D-35392 Giessen, Germany

Received: February 12, 2001; In Final Form: April 11, 2001

High-resolution (0.0018 cm^{-1}) infrared spectra have been recorded in the CF stretching region for 1,1,2,2-tetrafluoroethane and its d_2 and $^{13}C_2$ isotopomers. These bands are sufficiently intense to give useful gas-phase spectra at −100 °C in a 3 m cell. For each spectrum the rotational structure of the A/C-type and B-type bands due to the anti rotamer, which is a highly asymmetric rotor with $\kappa = -0.295$, have been analyzed. Rotational constants for a Watson-type Hamiltonian have been fitted for the common ground state of each isotopomer and the separate upper states. A complete structure for the nonpolar anti rotamer has been derived and compared with the structure of the polar gauche rotamer obtained from microwave spectroscopy. The geometric parameters for the anti rotamer are $r_{CH} = 1.087(5)$ Å, $r_{CC} = 1.511(4)$ Å, $r_{CF} = 1.359(7)$ Å, $\alpha_{CCH} = 112.9(3)°$, $\alpha_{CCF} = 108.5(6)°$, $\alpha_{FCF} = 107.4(6)°$, and $\tau_{FCCF} = 63.6(12)°$. The structural parameters for the two isomers of 1,1,2,2-tetrafluoroethane are compared with recent calculations, and trends in these parameters and those of the rotamers of 1,2-difluoroethane are discussed.

Introduction

This paper reports on an investigation of the structure of the anti rotamer of 1,1,2,2-tetrafluoroethane (TFEA) by high-resolution infrared spectroscopy in parallel with a recent determination of the structure of the gauche rotamer by microwave spectroscopy.[1] The microwave method was appropriate for the polar gauche rotamer, but infrared spectroscopy is needed for the nonpolar anti rotamer.

Interest in the complete structure of the two rotamers of TFEA arises from investigations of the puzzling gauche effect. The gauche effect is exhibited by the rotamers of 1,2-difluoroethane, for which the gauche rotamer has the lower energy despite the closer proximity of the electron-withdrawing fluorine atoms in the gauche rotamer than in the anti rotamer. As discussed in the previous paper, current qualitative theories that explain the gauche effect in 1,2-difluoroethane predict an even more compelling example of the gauche effect in TFEA.[1] Yet, experimental evidence shows that the anti rotamer of TFEA has a lower energy than the gauche rotamer by about 5 kJ/mol.[2] High-level calculations give energy relationships for the two fluoroethane rotamer pairs, in agreement with experimental observations.[3,4] The work of Muir and Baker provides comparisons of a wide range of computational models and favors density functional theory in the adiabatic connection method (ACM) with a triple-ζ, double-polarization (TZ2P) basis.[3] The work of Papasavva et al. uses the MP2/6-31G** model.[4] Having found that noticeable adjustments in bond lengths and bond angles accompany the change in conformation in 1,2-difluoroethane,[5] we embarked on a similar comparative study of the two rotamers of TFEA.

The investigation of the structure of the anti rotamer of TFEA by high-resolution infrared spectroscopy was regarded as a major challenge. The molecule is a highly asymmetric top with $\kappa = -0.295$ for the normal species, and all of the rotational constants are rather small for this type of investigation. Preliminary work by Stone et al. on the analysis of bands in the high-resolution infrared spectrum of TFEA suggested, however, that the analysis might be possible without the use of the jet-beam-expansion and diode-laser techniques, which were used in the initial study.[6] These workers had done a first analysis of the ν_{16} A/C-hybrid band due largely to asymmetric CF stretching and had obtained rotational constants for the ground state of the normal species. They had also shown, to their disappointment, that this band was unperturbed to the extent it was observable in their very low-temperature spectrum. For our purposes the lack of perturbations was an advantage.

Stone and co-workers investigated microwave spectra of the gauche rotamer of TFEA and its ^{13}C isotopomer in natural abundance.[6] From this work and previous electron diffraction studies,[7] they developed a partial structure for the gauche rotamer. These parameters for the gauche rotamer and a CC bond length in the anti rotamer based on the single set of rotational constants for this species led to a partial structure for the anti rotamer. These parameters were a useful starting point in the present investigation for computing rotational constants for the anti rotamer and its isotopomers.

For a determination of a complete structure of TFEA, it is, of course, necessary to analyze bands in the spectra of isotopically substituted modifications. Making the very large quantities of the isotopomers of TFEA needed for jet-beam infrared experiments seemed out of the question. On the other hand, the two CF stretching modes have very intense bands, and TFEA is rather volatile with a bp of −23 °C.[8] Thus, it seemed that useful spectra might be recorded at about −100

10.1021/jp010539z CCC: $20.00
Published on Web 05/19/2001

°C with modest amounts of material in the 3 m, coolable cell associated with the Bruker IFS 120 HR instrument in Giessen. We also hoped that the somewhat simplified spectrum at low temperature would be analyzable with the resolution of 0.0018 cm^{-1} available on the Bruker instrument. Contributions from the higher energy gauche rotamer would also be largely removed from the spectrum at −100 °C. Even with the simplification of a spectrum recorded at this temperature, we were concerned about the overlap of the P-branch of the B-type band for ν_8 with the R-branch of the A/C-type band for ν_{16}. We also doubted the usefulness of Loomis−Wood (LW) software for analyzing the rotational structure of a highly asymmetric top with $\kappa = -0.295$. All of these experimental issues proved to be manageable.

For the d_2 and $^{13}C_2$ isotopomers a synthesis was devised. These species were prepared by brominating commercially available acetylene-d_2 and acetylene-$^{13}C_2$ to give the tetrabromoethanes, which were reacted with AgF_2, as described fully elsewhere.[9]

The medium-resolution infrared and Raman spectra of TFEA and its isotopomers were fully investigated as a preliminary to the high-resolution investigation.[9] This study led to some revisions in the assignments of the normal modes of the rotamers of TFEA as well as to first assignments for the fundamentals of the isotopomers.

Because TFEA (Freon 134) may enter the atmosphere from use in refrigeration systems, extensive information about its high-resolution infrared spectrum is of use in monitoring its presence in the atmosphere. In a related study, Smith et al. measured the infrared absorption of TFEA with 0.03 cm^{-1} resolution at temperatures from 203 to 297 K and at pressures of 5, 20, and 100 kPa of air.[10] This work was done to assess the potential for TFEA to absorb in the infrared window in the atmosphere and contribute to greenhouse warming.

Experimental Section

Samples of the d_2 and $^{13}C_2$ isotopomers of TFEA in the millimole range were prepared and characterized as described elsewhere.[9] TFEA itself was a commercial sample (PCR, Gainesville, FL) and was used without further purification after checking its medium-resolution infrared spectrum.

High-resolution infrared spectra of TFEA and its isotopomers were recorded at Justus-Liebig-Universität in Giessen. The Bruker IFS 120 HR interferometer was equipped with a globar source, a Ge-coated KBr beam splitter, and a Ge:Cu detector operating at 4.2 K. To reduce the optical range to 900−1250 cm^{-1}, a filter was used. The resolution was (1/MOPD) 0.001 84 cm^{-1}. Samples for spectroscopy were contained in a 3.02 m cell cooled to −100 °C with a flow of cold nitrogen gas. For the spectrum of the normal species 70 scans were accumulated for a sample at a pressure of ∼0.1 mbar (hPa). For the d_2 species 160 scans were accumulated for a sample at a pressure of ∼0.2 mbar. For the $^{13}C_2$ species 140 scans were accumulated for a sample at a pressure of ∼0.03 mbar. Interferograms were zero-filled, and boxcar apodization was used. Transmission spectra were calibrated using OCS lines.[11]

Locating subband series in the dense rotational structure in bands of TFEA was greatly aided by use of the LW program developed in Giessen.[12] We were gratified that this program, which was written for use with linear, quasi-linear, and near-prolate tops, worked so well for the highly asymmetric tops of TFEA and its isotopomers. Ground-state combination differences (GSCDs) and spectral lines were fit to Watson-type Hamiltonians in the asymmetric rotor reduction and the I^r representation with a version of Dr. Arthur Maki's ASYM program. A related program, called ASYMBD, was used to predict spectral lines and intensities from rotational constants. Another program written by Christopher F. Neese in Visual Basic as an add-in to Microsoft Excel was very helpful in organizing predictions made with ASYMBD into subband series. This program also makes it easy to display simultaneously graphs of computed spectra and observed spectra within the spreadsheet environment. In the structure fitting work, Professor Richard Schwendeman's program, modified at the University of Michigan and known as STRFIT87, was used.

Results and Discussion

Selection Rules. The anti rotamer of TFEA has C_{2h} symmetry. Thus, the modes of the a_u and b_u symmetry species are infrared active. The *a* axis for the smallest principal moment of inertia passes through the center of symmetry, lies in the plane of symmetry of the molecule, and nearly bisects the lines between the pairs of fluorine atoms. The *c* axis for the greatest moment of inertia also lies in the symmetry plane. The *b* axis for the intermediate moment of inertia is perpendicular to the plane of symmetry. As a consequence of the orientations of the principal axes, the a_u modes, which are antisymmetric with respect to the plane of symmetry, produce B-type bands. The b_u modes, for which the oscillating dipole lies in the plane of symmetry, produce hybrid A/C-type bands. For the normal and the $^{13}C_2$ isotopomers of the anti rotamer of TFEA, the B-type band of interest corresponds to ν_8, and the A/C-type band corresponds to ν_{16}. For the d_2 species, the B-type band corresponds to ν_7, and the A/C-type band corresponds to ν_{15}.[13] For all three isotopomers both bands of interest are principally CF stretching modes and thus have high intensity.

The selection rules for rotational transitions are $\Delta J = 0, \pm 1$ for all transitions and $\Delta K_a = 0$, $\Delta K_c = \pm 1$ for A-type transitions, $\Delta K_a = \pm 1$, $\Delta K_c = \pm 1$ for B-type transitions, and $\Delta K_a = \pm 1$, $\Delta K_c = 0$ for C-type transitions.

Coriolis coupling is allowed between the a_u and b_u antisymmetric CF stretching modes because $a_u \times b_u = b_g$, which is the symmetry species of a rotation. Even though Coriolis coupling is allowed and the two frequencies are only 17 cm^{-1} apart for the normal species and slightly less for the $^{13}C_2$ species, no effects of Coriolis coupling were observed in the two bands of any of the isotopomers.

Analysis of the A/C-Type Band of TFEA. Figure 1 shows a survey of the high-resolution infrared spectrum of the CF stretching region of TFEA. Both bands are due to the anti rotamer. The lower frequency band with the Q-branch is the A/C-type band.

Getting started on the analysis of the A/C-type band relied on the assignment of Stone et al.[6] Because of the very low temperature in the jet-beam expansion, their analysis was, however, confined to the band center. Series did not extend very high in *J*, and gaps occurred because some of their diode lasers did not work properly. From their work, we were, however, certain of K_a'' and initial J'' assignments for several series. With the aid of LW displays (see below for examples), we were able to extend these series to much higher *J* values and to find other series with higher K_a'' values. All of these initial assignments were prolate-like, i.e., constant-K_a'' series, of the ^QR_K and ^QP_K type. These series were also "low-K_c" series for which $K_a'' + K_c'' = J''$. Figure 2 shows details of the assignments of prolate-like series for $^QP_0$ through $^QP_3$ in a 1.4 cm^{-1} region of the P-branch in the predominately A-type band of TFEA. The low-*J*

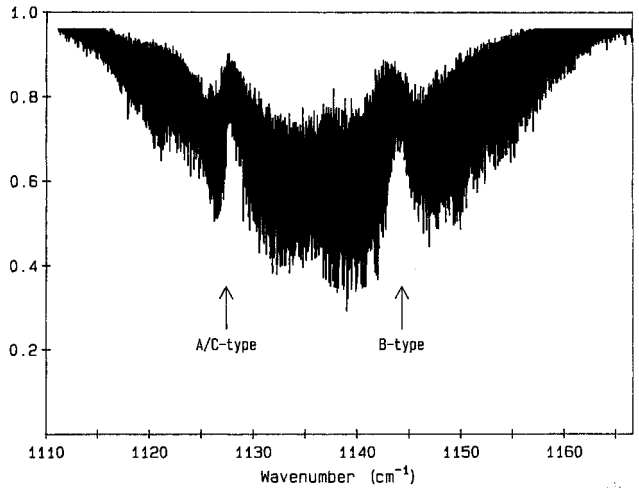

Figure 1. Survey of the high-resolution infrared spectrum of the two bands in the CF stretching region for the normal form of 1,1,2,2-tetrafluoroethane.

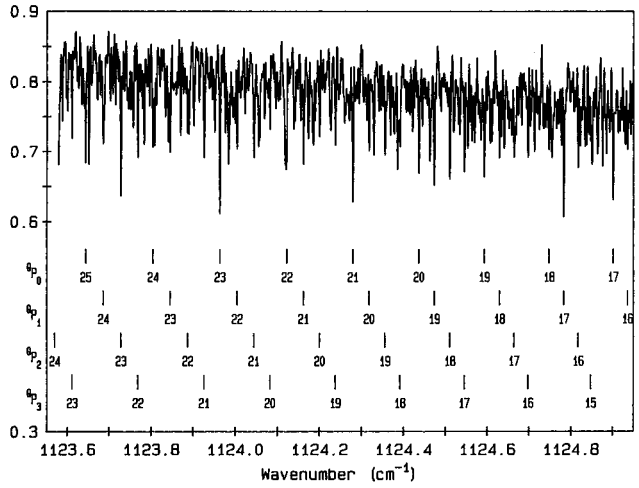

Figure 2. Detail of P-branch from A-type band of 1,1,2,2-tetrafluoroethane.

regions of the series, which consisted of rapid changes in the spacing between lines, were dubbed "serpentine" regions and, except for those lines already assigned by Stone et al., were assigned later.

With subband series assigned to the extent possible with the aid of LW displays, we computed GSCDs between corresponding R-branch and P-branch lines and fitted ground-state constants to a Watson-type Hamiltonian with a limited set of centrifugal distortion constants. GSCDs computed from those lines observed by Stone et al. but not by us were included in the fitting of ground-state constants. In doing so, we were careful to avoid redundant use of observed lines within a data set.[14] Then, the ground-state constants were held fixed while upper-state constants were fitted.

We used ASYMBD to predict frequencies and intensities for the lines in the serpentine region. Input to ASYMBD included ground-state and upper-state rotational constants and a temperature of 173 K. These predictions guided the search for low-K_c lines of reasonable intensity near the predicted frequencies. With low-K_c lines from the serpentine region added to the data set, new GSCDs were computed, and revised ground-state constants were fitted. On the basis of the updated ground-state constants and the augmented assignment of lines, new upper-state constants were fitted and "high-K_c" lines in the serpentine region were predicted. High-K_c series have $K_a'' + K_c'' = J'' + 1$. For

TABLE 1: Rotational Constants for the Anti Rotamer of 1,1,2,2-Tetrafluoroethane

	ground state[a]	ν_8 vibrational state[a,b]	ν_{16} vibrational state[a,b]
A/cm^{-1}	0.171 289 32(83)	0.171 699 57(11)	0.170 063 39(25)
B/cm^{-1}	0.105 022 4(11)	0.104 743 73(14)	0.104 907 05(16)
C/cm^{-1}	0.068 957 86(27)	0.069 148 510(37)	0.068 479 988(33)
κ	−0.295 142	−0.305 805	−0.282 939
$10^8\Delta_K$/cm^{-1}	4.84(25)	6.110(28)	3.07(12)
$10^8\Delta_{JK}$/cm^{-1}	−1.23(30)	0.993(28)	−2.78(14)
$10^8\Delta_J$/cm^{-1}	1.569(71)	1.8522(46)	1.307(13)
$10^8\delta_K$/cm^{-1}	1.44(19)	1.906(13)	1.240(39)
$10^9\delta_J$/cm^{-1}	5.32(35)	3.990(23)	6.831(65)
$10^{13}H_K$/cm^{-1}	0.0	1.43 (58)	0.0
$10^{12}H_{KJ}$/cm^{-1}	0.0	0.0	0.0
$10^{12}H_{JK}$/cm^{-1}	0.0	1.881(49)	0.0
ν_0/cm^{-1}		1144.339 220(23)	1127.434 477(25)
std dev/cm^{-1}	0.000 38	0.000 36	0.000 39
no. of lines[c]	1215	1668	1206
max. K_a''	36[d]	56[d]	10
max. J''	67	67	75

[a] Uncertainties in last two numbers are given in parentheses. [b] Ground-state constants were held fixed while upper-state constants were being fitted. [c] Number of GSCDs or lines used in the fitting. [d] In oblate-type series; 11 or 12 in prolate-type series.

the A-type transitions, the high-K_c series are $^{Q}R_K$ and $^{Q}P_K$. Guided by the predictions of frequencies and intensities made with ASYMBD, we looked for high-K_c lines in the serpentine regions. Beyond the serpentine region, a high-K_c series with a particular value of K_a'' joins a low-K_c series with K_a'' one unit less. This coalescence occurs at progressively higher J'' values as K_a'' increases. In each case, after the joining up occurs, only the low-K_c series was retained in the data set. With these added assignments in hand, augmented GSCDs were computed, improved ground-state constants were fitted again, and upper-state constants were fitted. For A-type transitions assignments extended to K_a'' values of 10 and J'' values as high as 67.

From their investigation of the A/C-type band, Stone et al. concluded that the A-type component was about 8 times more intense than the C-type component. Guided by predictions, we explored the possibility of adding to the assignments made by Stone et al. for the C-type component but found that relatively little could be done and then only near the band center. The number of C-type lines included in the data set is 39 for $^{P}Q_1$, 3 for $^{R}Q_0$, 19 for $^{R}P_0$, and 18 for $^{R}R_1$.

The final step in the assignment of the A-type component of the band was to work on the Q-branch after GSCDs from the B-type band had been incorporated in the data set (see below). Several oblate-type, low-K_c series in which $K_c'' = 0$, 1, and 2 were assigned in the Q-branch of the A-type component of the A/C-type band. Oblate-type series have K_c'' constant for the series. These Q-branch lines do not form accessible GSCDs with lines in the R- or P-branches because needed high-K_c R- and P-branch lines were not observed with confidence near the congested band center. In contrast to the spectrum recorded at −100 °C, the Q-branch structure of the A/C-type band is not apparent in the survey spectrum at room temperature. This lack of definition of the Q-branch in spectra at room temperature caused this spectral region to be misinterpreted in earlier studies.[2]

The total number of lines in the file for the A/C-type band is 1206. This file is supplied as supplementary Table 2S and includes the statistics of fitting the rotational constants. Supplementary Table 1S, which is discussed in the next section, contains the GSCDs. We shall defer discussing the constants for the rotational Hamiltonian, which are given in Table 1,

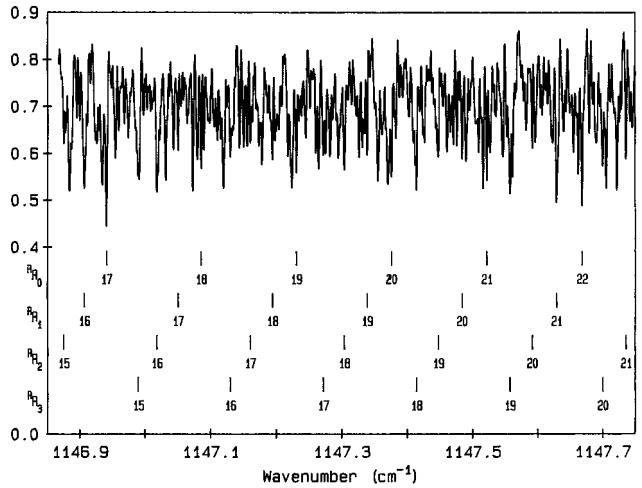

Figure 3. Detail of R-branch from B-type band of 1,1,2,2-tetrafluorethane.

because the final fitting of the constants depends on GSCDs derived from the B-type band as well as from the A/C-type band.

A careful comparison was made of the frequencies reported by Stone et al. for lines in the A/C-type hybrid band and also observed in the present work. No systematic difference was found even though the accuracy in the earlier work done with tunable diode lasers was higher.[6] Thus, for the investigation of the normal species, we incorporated GSCDs from the work of Stone et al. which were not observed in the present study. These lines were largely from the band center region, which was distinguished more cleanly in the cold-jet-beam, diode-laser experiments.

Analysis of the B-Type Band for TFEA. The ground-state rotational constants derived from the lines in the A/C-type band gave a good starting point for analyzing the B-type band of TFEA. With LW displays (see below for examples), prolate-type, low-K_c ${}^{R}R_K$ and ${}^{R}P_K$ series were readily found in the R- and P-branches and put into an ordered sequence within each branch. Thus, we had reasonable initial assignments for K_a'' values in each branch. The band centers for these subbands were, however, in doubt because of the serpentine regions between the initially assignable parts of the series and the centers of each subband. In addition, the overall center of the B-type band was, as judged from the overall scan, in doubt by a few tenths of a reciprocal centimeter. Thus, the J'' values for the subband series were in doubt.

To secure an assignment, we used a "notching" technique on a spreadsheet. GSCDs for a pair of K_a'''s were computed from the assignments for the A/C-type band and were put on a spreadsheet along with R-branch and P-branch series with the corresponding K_a'' values suspected of being mates with upper states in common. GSCDs computed from the observed lines were compared with the predicted values. The columns of R- and P-branch lines were moved up and down the spreadsheet relative to the GSCDs until observed and predicted GSCDs agreed. This technique was repeated with other K_a'' values to confirm assignments of the K_a'' values and to secure assignments of J'' values. Figure 3 shows details of the assignment of ${}^{R}R_0$ to ${}^{R}R_3$ in a 1.8 cm^{-1} interval of the R-branch in the B-type band of TFEA.

Further work on analyzing the serpentine regions near the center of the B-type band for low-K_c and high-K_c lines followed a similar method as described for the A-type lines in the other band. The high-K_c lines of significant intensity in the B-type component were ${}^{P}R_K$ and ${}^{P}P_K$ transitions. These series join low-K_c series with a K_a'' value one less. New data for GSCDs were added as progress was made. Predictions showed that intensities of high-K_c lines of ${}^{R}R_K$ and ${}^{R}P_K$ and low-K_c lines of ${}^{P}P_K$ and ${}^{P}R_K$ series are too weak to assign.

Assignments in the B-type band extended to K_a'' of 12 and to J'' values in the 60s for many series in the R-branch. Despite the overlap with series of the A/C-type band in the P-branch, J'' values were found as high in the P-branch as in the R-branch for prolate-type series. We predicted the frequencies and intensities of Q-branch transitions in subbands and found that these lines were too weak to observe in the available spectrum.

A number of oblate-type, low-K_c series with fixed values of K_c'' from 0 to 7 were assigned in the R- and P-branches of the B-type band. Oblate-type series have significantly different spacing than prolate-type series and thus appear with quite different parameter choices in a LW display (see below for an example). These series, which extend to K_a'' values as high as 56 and J'' values as high as 62, appreciably strengthen the data set. Oblate-type series appeared assignable up to $K_c'' = 13$. Extending these assignments seemed, however, of low value because a similar extension for the d_2 species made insignificant changes in the rotational constants. We predicted similar oblate-type series for the A-type band but concluded that these lines were too weak to observe.

Fitting the lines in the B-type band and the A/C-type band and finding common GSCDs for the two bands gave us high confidence that the assignments were correct for this very rich spectrum, which includes hot band series as well as lines from ground-state transitions. The analysis of the Q-branch of the A/C-type band was done after the full set of GSCDs had been found. Because the rate of change of spacing between Q-branch lines is great, our ability to fit these lines well is a further stringent test of the correctness of the assignment. As noted before, the Q-branch lines do not form accessible GSCDs with lines in the R- and P-branches of the A-type component of the A/C-type band.

Supplementary Table 3S gives the 1674 lines assigned in the B-type band and the statistics of fitting these lines to rotational constants. Supplementary Table 1S gives the 1215 GSCDs derived from both the B-type band and the A/C-type band. Included in the GSCDs are 229 values derived from the study of Stone et al.[6] These added values were nonredundant within the Stone et al. data set[13] and with respect to the observations made with the Bruker instrument. What appear to be redundant GSCDs with the same quantum numbers in Table 1S arise from the separate observations in the A/C-type and B-type bands. Table 1S also gives the statistics of fitting the ground-state rotational constants, which are, in turn, used in the fittings of the upper-state constants for the B-type and A/C-type bands, that is, ν_8 and ν_{16}, respectively. Table 1 contains the rotational constants for TFEA.

Stone et al. fitted ground-state constants to a much smaller data set.[6] They fitted the upper-state constants to a somewhat larger data set but substantially smaller than in the present work. For the ground state they obtained 0.171 283 5(22), 0.105 015 2(9), and 0.068 952 11(14) cm^{-1} for *A*, *B*, and *C*, respectively, without fitting any centrifugal distortion constants. For the upper state of the ν_{16} mode, they obtained 0.170 062 1(4), 0.104 890 8(3), and 0.068 473 1(3) cm^{-1} for *A*, *B*, and *C*, respectively, and $-4.94(50) \times 10^{-6}$ cm^{-1} for Δ_J. Under the circumstances of much larger data sets and the incorporation of more centrifugal distortion constants in the present work, these values are in good agreement with our new results. Although sextic centrifugal

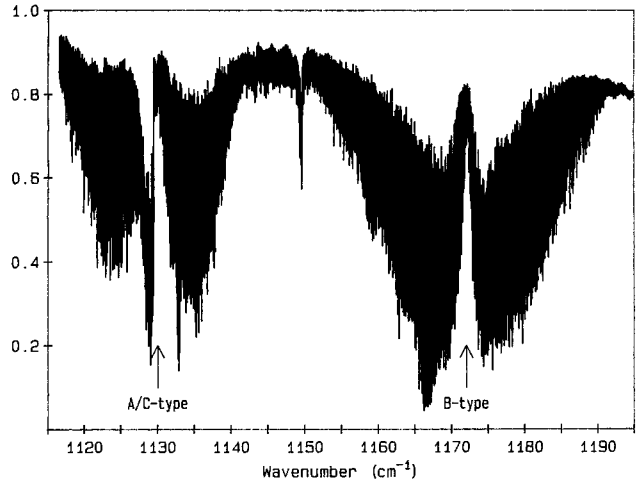

Figure 4. Survey of the high-resolution infrared spectrum of the two bands in the CF stretching region of 1,1,2,2-tetrafluoroethane-d_2.

constants were not used for the smaller data sets of GSCDs and of lines in the A/C-type band, they were needed to give a good fit to the larger data set for the B-type band. As reported in supplementary Tables 1S for the ground-state fitting, the correlation coefficient is unduly high between δ_J and Δ_J. This uncertainty has, however, a negligible effect on the A'', B'', and C'' constants which are of principal interest in this structural study.

Analysis of the Bands for TFEA-d_2. Figure 4 shows the high-resolution survey spectrum of the two bands for TFEA-d_2 in the CF stretching region. For this species the two bands are well-separated by almost 43 cm^{-1}. The center of the A/C-type band for ν_{15} at 1129.5 cm^{-1} is shifted only a little from that of the normal species at 1127.4 cm^{-1}. It is the ν_7 mode that has experienced a significant increase in frequency as mixing with the higher frequency CH bending mode has been replaced with what is probably less mixing with the lower frequency CD bending mode. This mixing interpretation is consistent with the relatively higher intensity of the B-type band than of the A/C-type band in the spectrum of the d_2 species compared to the intensities in the spectrum of the normal species. Also, the intensity of the a_u CH bending mode in the normal species is relatively strong, which is consistent with this mode gaining intensity by mixing with the a_u CF stretching mode. The weak feature at 1150 cm^{-1} between the two bands of interest in the spectrum of the d_2 species is assigned as $\nu_5 + \nu_{17}$, which is of B_u symmetry and predicted at 1147 cm^{-1}.

Getting started on the assignment for TFEA-d_2 was more challenging than for the normal species. In contrast to the normal species, no secure start on the assignment was available from the previous work. Ground-state rotational constants for the d_2 species were predicted from the geometric parameters found by Stone et al. and improved by scaling the rotational constants by the ratio of the observed and predicted constants for the normal species. These constants and ASYMBD gave predictions of GSCDs. Starting the assignment with the B-type band led to a misassignment of the J'' values by one unit. It was sobering to obtain a credible fit of ground-state and upper-state constants with this misassignment. Getting a good start on assigning the A-type component of the A/C-hybrid band was aided by knowing that the overall band center was just at the high-frequency edge of the well-defined Q-branch. After assigning the A-type component and revising the assignment for the B-type band, the excellent consistency of GSCDs derived from the two bands was strong evidence for the correct assignment of both bands.

Analysis of the A/C-Type Band for TFEA-d_2. Assigning the A-type component of the A/C-type band was begun by finding prolate-type series in the R- and P-branches with the aid of the LW program. Figure 5 shows an LW display of a number of these series in the R-branch of the A-type component of the A/C-type band. Series from $^{Q}R_0$ to $^{Q}R_6$ are shown crossing at a common point. Assigning the K_a'' values for these series in the R-branch was reasonably certain because, near the top of the display, the series start with progressively larger J values as the K_a'' values increase. Assigning the K_a'' values in the P-branch depended on recognizing a less obvious pattern for location of the subband series in the LW display. With the GSCDs derived from the approximate rotational constants, notching experiments were done to confirm K_a'' assignments and to find J'' values. Because the initial GSCDs were approximate, agreement between observed and predicted GSCDs of somewhat less than the relatively large value of 0.01 cm^{-1} was accepted. As an additional assignment aid, averaging frequencies with the same J'' values in the R- and P-branches gave a close approximation to the overall band center. Prolate-type series with higher K_a'' values were found and the initial series were extended to higher J'' values with the aid of predictions made from the rotational constants. Values for K_a'' extended to 12, and J'' reached 74. With a limited number of prolate-type series assigned, the correlation coefficient between the fit of the A and B rotational constants was quite high. This correlation decreased significantly as the data set grew.

The clue to the errant initial assignment for the B-type band was lack of agreement of GSCDs for the two band types. The assignment for the B-type band was adjusted to bring the GSCDs from this band into agreement with those from the A/C-type band within experimental error. GSCDs from both bands were used in fitting ground-state rotational constants and, in turn, fitting upper-state rotational constants for the A/C-type band.

Analysis of lines near the band center in the serpentine regions of subbands was done with the aid of predictions made from updated rotational constants. Extensions of the low-K_c series were found first. High-K_c lines, which join low-K_c series having K_a'' values 1 less, were also found in the serpentine regions with the aid of predictions.

After the B-type band had been analyzed and lines from oblate-type series extending to high K_a'' values had been incorporated into the GSCD file, the Q-branch of the A/C-type band was investigated. Oblate-type series in the Q-branch with K_c'' extending from 0 to 2 were assigned. These Q-branch transitions do not form GSCDs with assignable lines in the R- and P-branches and thus could not be confirmed with GSCDs. However, a prediction of the spectrum in the Q-branch gives excellent agreement with the observed spectrum. This agreement is shown in Figure 6. The agreement between the spectrum predicted for A-type transitions in the Q-branch and the observed spectrum in this region is strong evidence that C-type transitions contribute little intensity to the A/C-type band for TFEA-d_2. We also predicted C-type transitions and confirmed that these lines made very small contributions.

For TFEA-d_2 the Q-branch of the A/C-type band is much more compact than the Q-branch of the normal species. This difference is due to the smaller change in rotational constants between the ground state and upper state for the d_2 species than for the normal species. In addition, the spectrum of the normal species appears to have a larger contribution of intensity from C-type lines in the band center.

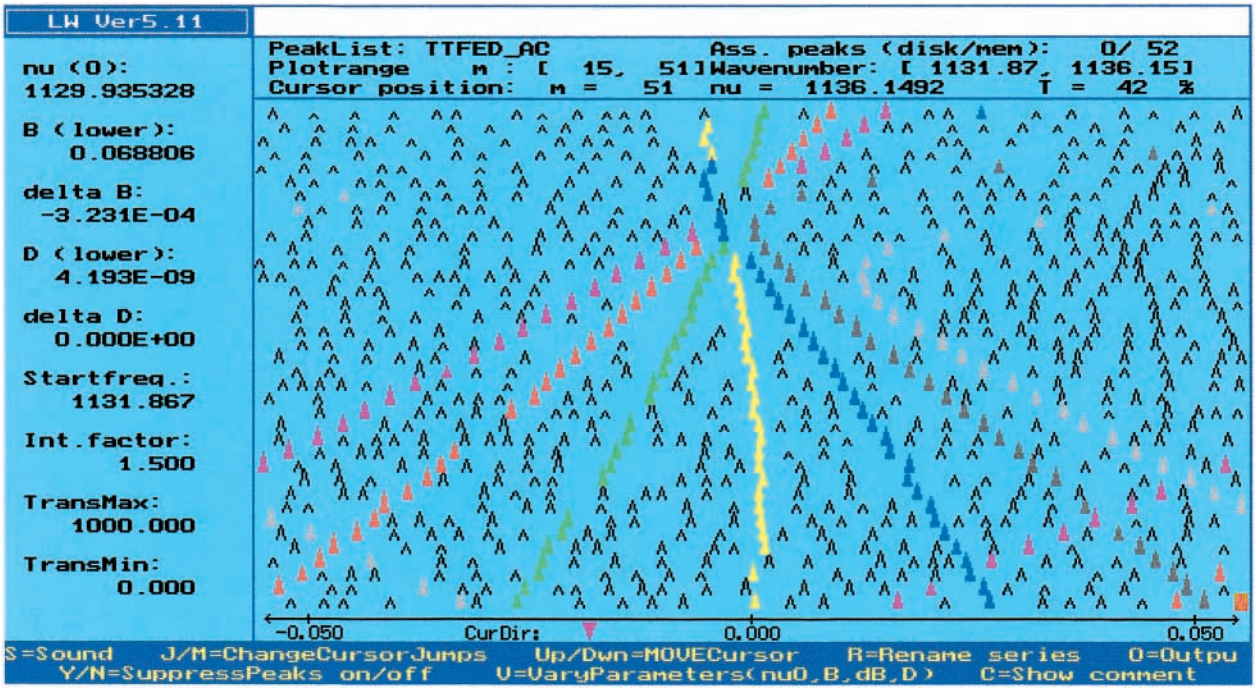

Figure 5. Loomis−Wood display of prolate-type series in the R-branch of the A-type band of 1,1,2,2-tetrafluoroethane-d_2. Series shown are $^{Q}R_0$ (magenta), $^{Q}R_1$ (orange), $^{Q}R_2$ (green), $^{Q}R_3$ (yellow), $^{Q}R_4$ (blue), $^{Q}R_5$ (brown), and $^{Q}R_6$ (pink).

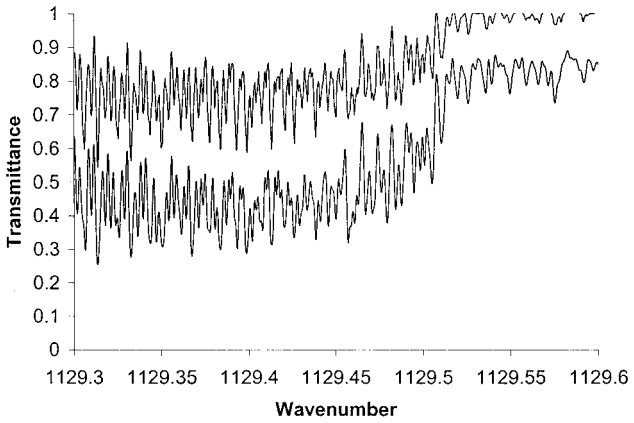

Figure 6. Comparison of the observed (lower trace) and calculated Q-branch structure in the A-type band of 1,1,2,2-tetrafluoroethane-d_2.

A total of 1283 GSCDs derived from the two bands for the CF stretching modes of TFEA-d_2 are given in supplementary Table 4S. Statistics of fitting the ground-state rotational constants are part of this table. Table 2 gives the rotational constants fitted to the GSCDs. Supplementary Table 5S gives the 1354 A-type transitions assigned for the A/C-type band of TFEA-d_2 and includes the statistics of fitting the upper-state rotational constants. Table 2 contains the resulting upper-state rotational constants.

Analysis of the B-Type Band for TFEA-d_2. The assignment of the B-type band was interwoven with the analysis of the A/C-type band, as described above. In the P-branch, prolate-type, low-K_c series were readily found and indexed with K_a'' values because these series crossed near a single point similar to the observation for the R-branch series of A-type transitions shown in Figure 5. Assigning the K_a'' values for prolate-type series in the R-branch of the B-type band depended on recognizing a different left-to-right pattern among the series in an LW display. Notching experiments on a spreadsheet with GSCDs derived from the A/C-type band gave assignments of K_a'' and J'' values. The method for extending the series into the serpentine region was the same as described for the normal species. Values for K_a'' extended to 10, and J'' reached 72.

TABLE 2: Rotational Constants for the Anti Rotamer of 1,1,2,2-Tetrafluoroethane-d_2

	ground state[a]	ν_7 vibrational state[a,b,c]	ν_{15} vibrational state[a,b]
A/cm^{-1}	0.164 443 68(49)	0.164 268 48(12)	0.163 991 77(34)
B/cm^{-1}	0.101 965 6(14)	0.101 720 09(21)	0.101 880 82(14)
C/cm^{-1}	0.068 742 35(30)	0.068 812 628(79)	0.068 405 790(33)
κ	−0.305 709	−0.310 520	−0.299 583
$10^8\Delta_K$/cm^{-1}	4.53(17)	5.626(37)	5.15(17)
$10^8\Delta_{JK}$/cm^{-1}	−1.85(23)	−3.235(46)	−2.60(17)
$10^8\Delta_J$/cm^{-1}	1.649(63)	2.077(12)	1.731(14)
$10^8\delta_K$/cm^{-1}	1.68(17)	4.161(36)	1.575(46)
$10^9\delta_J$/cm^{-1}	5.79(30)	4.966(66)	6.480(68)
$10^{13}H_K$/cm^{-1}	0.0	336(72)	0.0
$10^{12}H_{KJ}$/cm^{-1}	0.0	−46.2(98)	0.0
$10^{13}H_{JK}$/cm^{-1}	0.0	118(24)	0.0
$10^{13}H_J$/cm^{-1}	0.0	8.48(30)	0.0
ν_0/cm^{-1}		1172.128 767(27)	1129.517 823(25)
std dev/cm^{-1}	0.000 39	0.000 36	0.000 38
no. of lines[d]	1283	1936	1354
max. K_a''	50[e]	52[e]	12
max. J''	69	72	74

[a] Uncertainties in last two numbers are given in parentheses. [b] Ground-state constants were held fixed while upper-state constants were being fitted. [c] In addition, $h_J = 7.27 \times 10^{-13}$ (22) and $h_K = 5.06 \times 10^{-11}$ (12) cm^{-1}. [d] Number of GSCDs or lines used in the fitting. [e] In oblate-type series; 10 or 13 in prolate-type series.

Obvious clusters of lines extending far out in the R-branch were a strong indicator of assignable oblate-type series. Finding oblate-type series in the B-type band was, however, a challenge despite experience making similar assignments for the normal species. Careful exploration of LW display parameters succeeded. Figure 7 is an LW display showing a number of oblate series in the R-branch of the B-type band. The series with even K_a'' values from 0 to 8 cluster on the left of the display, and the series with odd K_c'' values from 1 to 9 cluster on the right. As seen in the upper left of the LW display, the effective B value for these oblate-type series is close to the A rotational

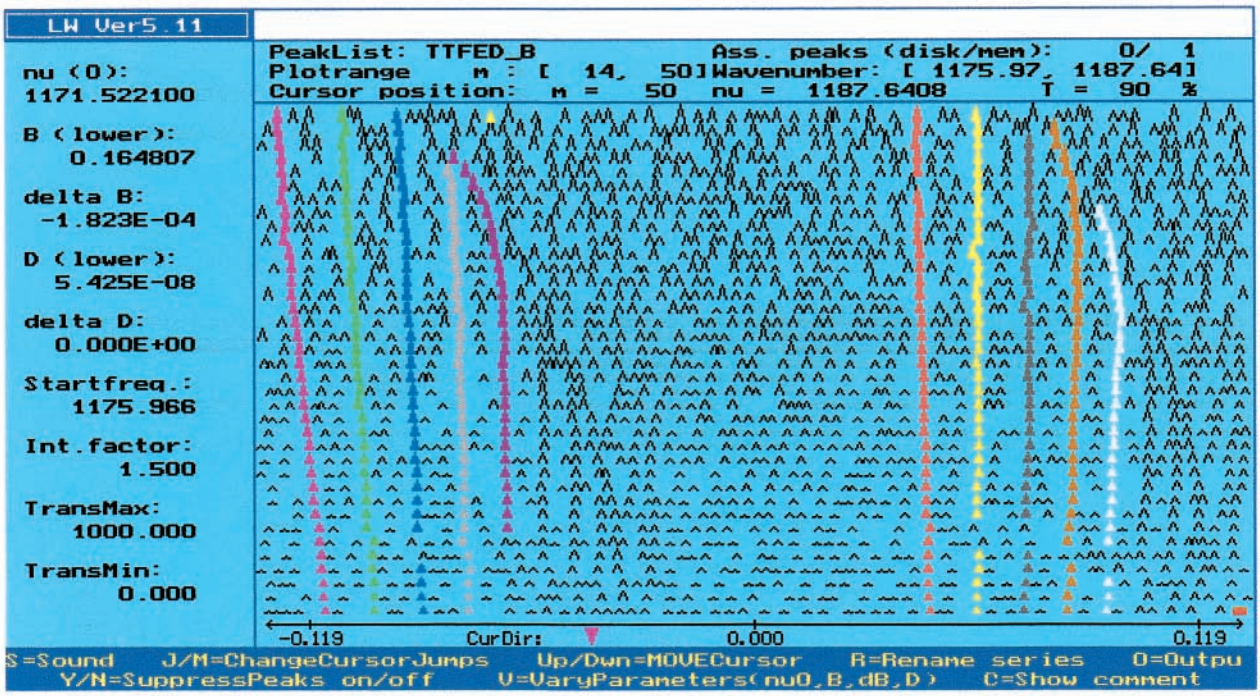

Figure 7. Loomis−Wood display of oblate-type series in the R-branch of the B-type band of 1,1,2,2-tetrafluoroethane-d_2. Series shown are ${}^{R}R_{0K_c}$ (magenta), ${}^{R}R_{1K_c}$ (orange), ${}^{R}R_{2K_c}$ (green), ${}^{R}R_{3K_c}$ (yellow), ${}^{R}R_{4K_c}$ (blue), ${}^{R}R_{5K_c}$ (brown), ${}^{R}R_{6K_c}$ (pink), ${}^{R}R_{7K_c}$ (tan), ${}^{R}R_{8K_c}$ (purple), and ${}^{R}R_{9K_c}$ (white).

constant, whereas the effective B value for prolate-type series, as shown in Figure 5, is close to C. Oblate-type series were assigned up to K_c'' of 15 in the R-branch and up to K_c'' of 13 in the P-branch. We predicted intensities for lines in Q-branches of the B-type band and concluded that these lines were too weak to observe near the congested band center.

A total of 1283 GSCDs derived from the B-type band and the A/C-type band of TFEA-d_2 are in supplementary Table 4S. Supplementary Table 6S gives the 1936 lines assigned in the B-type band and the statistics of fitting the upper-state rotational constants for ν_7. Table 2 gives the rotational constants for this upper state. To accommodate the data set of 1936 lines, including the high-K_a values from the assignment of oblate series for the B-type band of the d_2 species, a full set of sextic constants was employed, including h_J and h_K. For the ground-state fitting high correlation coefficients occurred between δ_J and Δ_J and between Δ_{JK} and Δ_K. These correlations have a negligible effect on the fitting of the principal rotational constants of the ground state.

Analysis of the Bands for TFEA-$^{13}C_2$. Figure 8 shows the high-resolution survey spectrum of the CF stretching region in the infrared spectrum of TFEA-$^{13}C_2$. As for the normal species, the two bands are overlapped. The substitution of ^{13}C has shifted both bands to lower frequency by almost the same amount, about 25 cm^{-1}. In addition, the intensity of the CF stretching region is about twice as strong for the $^{13}C_2$ species as for the normal species. The increased intensity for the CF stretching bands of the $^{13}C_2$ species has been attributed to a reduced mixing of the symmetry coordinates for antisymmetric CH bending and antisymmetric CF stretching.[9] For the normal species, bands for the CH bending modes gain intensity at the expense of the CF stretching modes. The Q-branch for the A/C-type band is comparable to the broadened shape in the spectrum of the normal species and decidedly less distinct than for the d_2 species.

Drawing on experience with the d_2 species, we started the analysis of the rotational structure of the $^{13}C_2$ species with the A/C-type band and approximate rotational constants, derived as described for the d_2 species, from the model of Stone et al.[6]

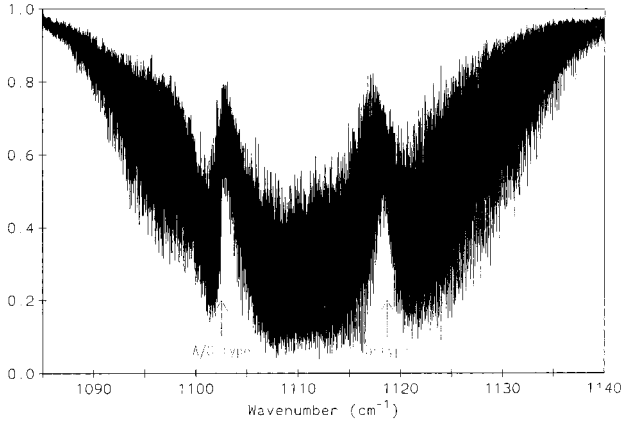

Figure 8. Survey of the high-resolution infrared spectrum of the two bands in the CF stretching region of 1,1,2,2-tetrafluoroethane-$^{13}C_2$.

In general, the analysis of the A-type component of the A/C-type band proceeded as described for the spectrum of the d_2 species. Figure 9 shows an LW display of prolate-type, low-K_c subbands in the R-branch of the A-type band. These series include lines from the serpentine region seen curving sharply away from the "linear" sequences. Shown are series ${}^{Q}R_0$ to ${}^{Q}R_5$. Prolate-type series in the P-branch were harder to index because of a more complicated pattern with no common crossing region. Notching experiments gave consistent assignments between the R- and P-branches. Values for K_a'' extended to 10, and values for J'' reached 73.

After the B-type band had been assigned and GSCDs had been found for the two bands, we analyzed the Q-branch of the A/C-type band. Oblate-type series from K_c'' of 0 to 4 and a scattering of higher values were assigned. Figure 10 shows separately computed A-type and C-type contributions to the Q-branch. The relative intensities of the A-type and C-type lines are estimates to account for the observed spectrum. The C-type contribution is clearly weaker. After attempting to do so, we made no assignments for the weak C-type transitions in the A/C-

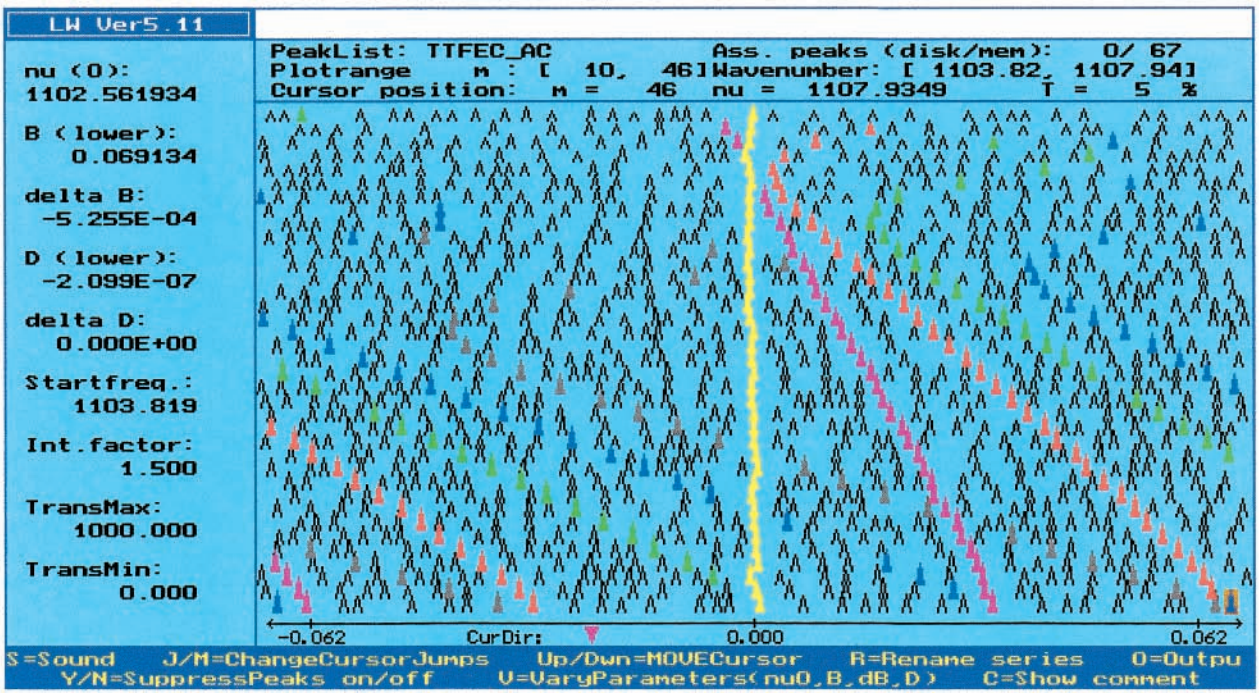

Figure 9. Loomis−Wood display of prolate-type series fit in the R-branch of the A-type band of 1,1,2,2-tetrafluoroethane-$^{13}C_2$. Series shown are $^{Q}R_0$ (yellow), $^{Q}R_1$ (magenta), $^{Q}R_2$ (orange), $^{Q}R_3$ (green), $^{Q}R_4$ (blue), and $^{Q}R_5$ (brown). Unassigned series to the left of $^{Q}R_0$ are believed to be from a hot band.

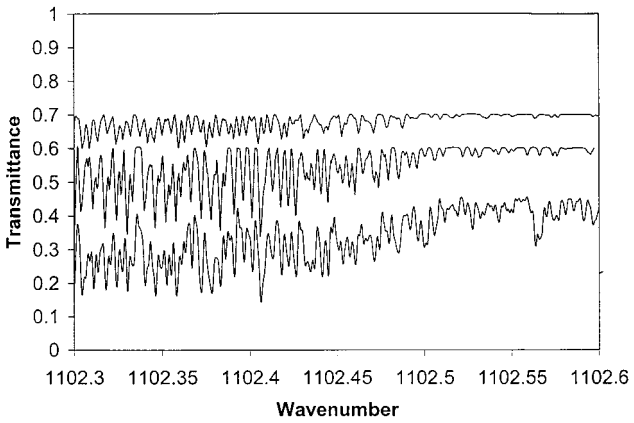

Figure 10. Comparison of the observed (lowermost trace) and calculated Q-branch structure in the A/C-type band of 1,1,2,2-tetrafluoroethane-$^{13}C_2$. The uppermost trace is an estimate of the contribution of the C-type component; the middle trace is an estimate of the contribution of the A-type component.

type band for the $^{13}C_2$ species. The additional lines between 1102.5 and 1102.6 cm^{-1} are presumably due to hot band contributions.

In general, the assignment of the rotational structure in the B-type band depended on finding prolate-type, low-K_c series in LW displays, using experimental GSCDs from the A-type band, and doing notching experiments. Extending low-K_c series into the serpentine region and finding high-K_c series in this region proceeded as described for the normal species. Series extended to K_a'' of 10 and J'' of 76. Assignments for oblate-type series in the B-type band extended from K_c'' of 0 to 13 in the R-branch. Because of overlap with the A/C-type band in the P-branch, series only up K_c'' of 7 were assigned in the P-branch.

Supplementary Table 7S gives the 1098 GSCDs derived from the A-type and B-type transitions along with the statistics of fitting the ground-state rotational constants. Supplementary

TABLE 3: Rotational Constants for the Anti Rotamer of 1,1,2,2-Tetrafluoroethane-$^{13}C_2$

	ground state[a]	ν_8 vibrational state[a,b]	ν_{16} vibrational state[a,b]
A/cm^{-1}	0.170 916 1(11)	0.171 315 70(13)	0.169 718 53(48)
B/cm^{-1}	0.104 278 6(13)	0.104 004 80(14)	0.104 158 18(21)
C/cm^{-1}	0.068 706 18(28)	0.068 909 322(65)	0.068 219 641(70)
κ	−0.303 935	−0.314 584	−0.291 968
$10^8\Delta_K$/cm^{-1}	5.84(31)	6.947(30)	6.80(14)
$10^8\Delta_{JK}$/cm^{-1}	−2.16(35)	0.165(32)	−4.973(89)
$10^8\Delta_J$/cm^{-1}	1.714(79)	2.0618(66)	1.278(10)
$10^8\delta_K$/cm^{-1}	1.70(21)	2.410(18)	0.895(63)
$10^9\delta_J$/cm^{-1}	5.97(39)	4.190(30)	7.331(50)
$10^{13}H_K$/cm^{-1}	0.0	−18.5(14)	253(14)
$10^{12}H_{KJ}$/cm^{-1}	0.0	3.27(23)	−17.0(13)
$10^{13}H_{JK}$/cm^{-1}	0.0	5.24(11)	−7.6(17)
$10^{13}H_J$/cm^{-1}	0.0	1.97(47)	−1.838(64)
ν_0/cm^{-1}		1118.662 535(23)	1102.505 360(30)
std dev/cm^{-1}	0.000 41	0.000 34	0.000 40
no. of lines[c]	1098	1833	1465
max. K_a''	33[d]	51[d]	10
max. J''	71	76	73

[a] Uncertainties in last two numbers are given in parentheses. [b] Ground-state constants were held fixed while upper-state constants were being fitted. [c] Number of GSCDs or lines used in the fitting. [d] In oblate-type series; 10 in prolate-type series.

Table 8S gives the 1465 A-type transitions observed and the statistics of fitting the rotational constants for the first excited state of the ν_{16} fundamental. Supplementary Table 9S gives the 1833 spectral lines assigned in the B-type band and the fitting of the upper-state constants for ν_8. Table 3 gives the rotational constants for the ground state and the first excited states of ν_8 and ν_{16}. In the fitting of the ground-state constants for the $^{13}C_2$ species the correlation coefficient between δ_J and Δ_J is quite large, but none of the correlation coefficients with the principal rotational constants is of significant size.

Structure Fitting. Structure fitting for the anti rotamer of TFEA was done by two procedures. The first procedure was a two-step process. First, the Cartesian coordinates for the carbon

TABLE 4: Cartesian Coordinates for *anti*-1,1,2,2-Tetrafluoroethane in the Principal Axis System

atom	*a*/Å	*b*/Å	*c*/Å
carbon[a]	±0.67390	0.0	±0.34124
hydrogen[a]	±0.59852	0.0	±1.42577
fluorine[b]	±1.36527	±1.09534	∓0.06966

[a] Substitution coordinates from Kraitchman analysis. [b] From fitting to moments of inertia with carbon and hydrogen Cartesian coordinates held at substitution values.

and hydrogen atoms were found from the three sets of moments of inertia with the double substitution relationships.[15] These Cartesian coordinates are given in Table 4. With the Cartesian coordinates for the HCCH array held fixed, the Cartesian coordinates for the fluorine atoms were found by fitting simultaneously to the nine rotational constants with STRFIT. In this fitting process the coordinates were constrained to C_{2h} symmetry. Thus, the HCCH torsional angle was set to 180.0°, and the four fluorine atoms were made equivalent, as were the hydrogen atoms and the carbon atoms. The Cartesian coordinates for the fluorine atoms from this two-step procedure are in Table 4 along with the substitution coordinates for the carbon and hydrogen atoms. The second procedure involved finding the coordinates of all three types of atoms in a global-fitting procedure with STRFIT. Once again, full C_{2h} symmetry was imposed on this calculation.

Table 5 gives the geometric parameters found for the anti rotamer of TFEA by the two fitting procedures, the substitution parameters for the carbon and hydrogen atoms supplemented by adjusted parameters for the fluorine atoms, designated r_s/r_0, and the global-fitted structure, designated r_0. Included with the r_s/r_0 parameters are the Costain uncertainties. The corresponding Costain uncertainties for the r_0 structure are essentially the same and are thus not given. Because the agreement between the geometric parameters found by the two procedures is very good, we have confidence in the resulting r_s/r_0 structure, which we prefer for the anti rotamer of TFEA. Table 5 includes comparisons with structural parameters found by the recent DFT and ab initio calculations[3,4] and by an electron diffraction study.[7] The one significant difference in comparison with the electron diffraction results, the CCH angle, can be attributed to the difficulty in finding weakly scattering hydrogen atoms by the electron diffraction method.

Table 5 also gives the microwave structure for the gauche rotamer[1] and comparisons with the calculated geometric parameters for this rotamer.[3,4] Geometric parameters for the gauche rotamer were not reported separately in the electron diffraction investigation because, other than for HCCH torsional angle, the parameters were taken to be the same as for the anti rotamer.[7] In the electron diffraction study it was difficult to distinguish contributions from the gauche rotamer, which was only about 16% of the mixture, from those of the dominant anti rotamer.

Figure 11 gives Newman projections for the two rotamers of TFEA. The projection for the anti rotamer is Figure 11a; the projection for the gauche rotamer is Figure 11b. The 2-fold symmetry axis of the gauche rotamer is shown with the dashed line, and the two different types of fluorine atoms in this rotamer are distinguished as sub-a and sub-g. The "a" designation refers to fluorine atoms anti to the hydrogen atoms, and the "g" designation refers to the fluorine atoms gauche to the hydrogen atoms. The sub-a fluorine atoms are closer to the C_2 axis.

Muir and Baker's comprehensive study of the structures and energetics of the whole range of fluorine-substituted ethanes is a valuable resource for ab initio results at various levels of theory and for a summary of experimental data as well.[3] In the following discussion of trends in geometric parameters, we quote data from this source. Furthermore, the ACM/TZ2P-basis results reported by Muir and Baker do not differ greatly from the MP2 results of Papasavva et al.[4] In the following discussion, we refer to the geometric parameters of the r_s/r_0 experimental structure.

Of course, exact agreement between the experimental results and calculations is not expected due to approximations in the models used in the calculations and due to the comparison of an equilibrium structure from the calculations with a ground-state structure from spectroscopy. A more favorable test of agreement is to compare trends in structural *differences* between the rotamers as reflected in the calculations and in the observations. The calculated CC bond lengths in TFEA are essentially the same for the each of the rotamers and so are the observed CC bond lengths. Both the CF_g bond lengths and the CCF_g bond angles, which are anti to each other in the gauche rotamer, as defined in Figure 11a, are calculationally and experimentally similar to the corresponding parameters in the anti rotamer. The F_a atoms in the gauche rotamer, as defined in Figure 11b, are distinctly different from the fluorine atoms in the anti rotamer, having only gauche relationships to fluorine atoms on the other carbon atom. The CF_a and CCF_a parameters in the gauche rotamer differ from those of the F_g atoms in this rotamer and the fluorine atoms in the anti rotamer in the same sense for both the calculations and for the experiment. Because the FCF bond angle in the structure fitting for the gauche rotamer was assumed from the ACM calculation, comparing changes in the experimental and predicted FCF bond angles for the two rotamers is questionable. For the CH bond lengths, the calculation predicts no difference between the rotamers, yet the experiment gives a CH bond that is 0.017(9) Å longer in the gauche rotamer. It is likely that the experimental result is influenced by the substantial anharmonicity in CH bond stretching. For the CCH bond angle in the gauche rotamer, the experimental result is 0.5(8)° smaller and the ACM result is 1.1° smaller in comparison with the anti rotamer. Thus, in going from the anti to the gauche rotamer, the CCH bond angle decreases in both the experimental results and in the calculation. The difference between these decreases is probably not significant given the uncertainty in the experimental value.

In the experimental results significant differences were found in torsional angles for anti and gauche TFEA, as shown in Figure 11. Torsional angles were, however, not reported from the DFT study. We discuss the differences in torsional angles below.

Complete structures for the two rotamers of 1,2-difluoroethane (DFEA),[5,16] which are summarized in Figure 12, and the new results for the two rotamers of TFEA provide a first opportunity to consider trends in observed geometric parameters for both rotamers due to increased, symmetric fluorine substitution in ethane. It is known that successive substitution of fluorine on one of the carbon atoms in ethane decreases the CC bond length compared to ethane, as does single substitution on both carbon atoms in DFEA.[3] Additional symmetric fluorine substitution causes the CC bond length to increase. Whereas the CC bond length in CH_3CF_3 is only 1.494 Å in comparison with the CC bond length in ethane of 1.535 Å, the CC bond length in perfluoroethane is 1.545 Å. The observations for DFEA and TFEA fit this overall pattern. In going from DFEA to TFEA the average CC bond length of the rotamers increases from 1.495 to 1.510 Å. The shortening of the CC bond due to fluorine substitution on one carbon atom is regarded as a consequence of a greater σ (more sp-like) character in the CC bond as the electronegative fluorine atom brings out more p character in the orbitals used by the carbon atom to make CF bonds. On the

TABLE 5: Geometric Parameters for *anti*- and *gauche*-1,1,2,2-Tetrafluoroethane[a]

	r_{CH}	r_{CC}	r_{CF}	α_{CCH}	α_{CCF}	α_{FCF}	τ_{HCCH}	τ_{FCCF}
				Anti Rotamer				
present work								
r_s/r_0[b]	1.087(5)	1.511(4)	1.359(7)	112.9(3)	108.5(6)	107.4(6)	180.0	63.6(12)
r_0[c]	1.091	1.504	1.360	113.1	108.7	107.3	180.0	63.5
MB calcd[d]	1.092	1.526	1.354	112.1	108.8	108.4	180.0	
PIK calcd[e]	1.089	1.513	1.363	112.0	108.3	108.8	180.0	
electr diffr[f]	1.098(6)	1.518(5)	1.350(2)	110.3(10)	108.2(3)	107.3(3)	180.0	
				Gauche Rotamer				
r_s/r_0[g]	1.104(4)	1.508(4)	1.348(5)[h]	112.4(3)	110.1(3)[h]	108.7[j]	65.2(7)	51.9(8)[h]
			1.359(4)[i]		109.1(4)[i]			67.3(6)[k]
MB calcd[d]	1.092	1.528	1.348[h]	111.0[l]	110.5[h]	108.7	67.4	
			1.357[i]		108.6[i]			
PIK calcd[e]	1.089	1.515	1.359[h]	112.0	109.2[h]	109.0		
			1.365[i]		108.1[i]			

[a] Bond lengths in Å; bond angles in degrees. [b] The C and H Cartesian coordinates were constrained to the r_s values, while the fluorine coordinates were fitted. Costain uncertainties in parentheses. [c] Unconstrained. [d] Muir and Baker.[3] [e] Papasavva, Illinger, and Kenny.[4] [f] Brown and Beagley.[7] [g] Reference 1. [h] Fluorine atoms (F_a) closer to the C_2 axis; supplements ref 1. [i] Fluorine atoms (F_g) farther from the C_2 axis; supplements ref 1. [j] This angle was taken from the DFT calculations and held at this value. [k] Between the two kinds of fluorine atoms. [l] This value was misreported in ref 1.

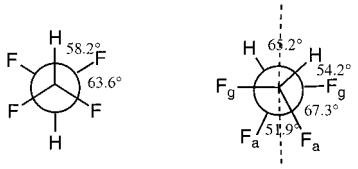

a b

Figure 11. Newman projections of the anti (a) and gauche (b) rotamers of 1,1,2,2-tetrafluoroethane. For the gauche rotamer, the direction of the 2-fold symmetry axis is shown with the dashed line. Torsional angles are also given. The nonbonded F···F distances are 2.734 Å in the anti rotamer and 2.797 Å (F_gF_a) and 2.673 Å (F_aF_a) in the gauche rotamer.

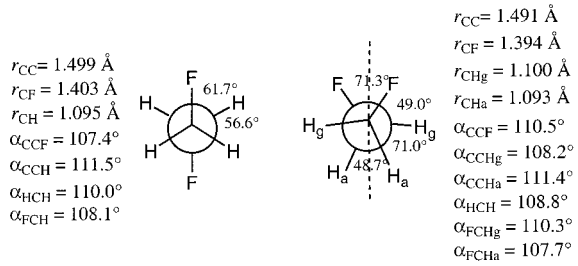

a b

Figure 12. Newman projections of the anti (a) and gauche (b) rotamers of 1,2-difluoroethane. See also the caption for Figure 11. The nonbonded F···F distance in the gauche rotamer is 2.897 Å.

other hand, fluorine substitution on both carbon atoms contributes nonbonded repulsion and bent bonding, as described by Wiberg.[17] These effects lead to weakening and lengthening of the CC bonds. The increase in the CCF bond angles in going from the anti to the gauche rotamer in both DFEA and TFEA also reflects additional FF repulsion in the gauche rotamers. The FCF bond angle appears to be less than the tetrahedral angle of 109.5° in both rotamers of TFEA in accord with the greater p character of the carbon orbitals used in the CF bonds. This comment is qualified because the FCF angle in the gauche rotamer was not fully determinable in the microwave investigation.

Successive fluorine substitution on a single carbon atom leads to significant CF bond shortening. This trend, which is explained with CF double bond character in nonbond resonance,[18] is also observed in going from DFEA to TFEA. The average CF bond length of 1.398 Å in DFEA decreases to an average CF bond length of 1.355 Å in TFEA.

For the most part the structural differences between the two rotamers of DFEA and the two rotamers of TFEA can be understood as a dominant influence of FF repulsion and a corresponding impact on torsional angles and bond angles. For this analysis we need some additional information that has not been published. The HCCH and HCCF dihedral angles, which are the torsional angles, for the gauche rotamer of DFEA were not reported by Takeo et al.[16] Therefore, we computed the two HCCH angles by the substitution method from the reported rotational constants.[19] The HCCF torsional angle came from differences of the other torsional angles. The various torsional angles for the two rotamers of DFEA are given in Figure 12. The other parameters, which are included in Figure 12, are the corresponding "r_s" parameters.[16] We have also computed the F···F nonbonded distance from the published parameters.[20] It is 2.897 Å. Torsional angles for the anti rotamer of DFEA, which were omitted from our previous paper,[5] are also supplied here.[21]

We consider the two rotamers of DFEA first, as shown in Figure 12. For the gauche rotamer of DFEA, the FCCF torsional angle is 71.3°, which is substantially greater than the default angle of 60°. Because the fluorine atoms in the two CFH_2 groups in the gauche rotamer rotate away from each other around the CC axis to relieve FF repulsion, the H_aCCH_a torsional angle opposite to the FCCF torsional angle is reduced to 48.7° as is the $FCCH_g$ angle decreased to 49.0°. The two H_aCCH_g angles are increased to 71.0°. The increased repulsion between the two CH_a bonds is relieved by an increase in the CCH_a bond angle to 111.4° relative to the sp^3 angle of 109.5°. Also the FCH_a bond angle is decreased some to 107.7°, whereas the H_aCH_g angle of 108.8° remains closer to the tetrahedral angle. Because of increased p character in a CF bond orbital caused by the electronegativity of the fluorine atom, a value of less than 109.5° is expected for the CCF bond angle. Thus, the enlarged CCF angle of 110.5° is further evidence of a response to FF repulsion.

Another way to see that a counter-rotation of the CFH_2 groups, as distinct from adjustments within these groups, occurs around the CC bond in the gauche rotamer of DFEA to relieve FF repulsion is to consider the projected angles of the CFH_2 group. The projected angles are found by summing appropriate dihedral angles. The projections of the two HCF angles and the one HCH angle on a plane perpendicular to the CC bond are 120.0°, 120.3°, and 119.7°, respectively. That these angles

are all close to 120° supports the adjustment-by-rotation intepretation.

For the anti rotamer of DFEA, the CCF bond angle is only 107.4°. This angle is consistent with extra p character in the CF bond orbital. The CCH bond angle is correspondingly large at 111.5°. Thus, the two CFH_2 groups, as a whole, rock inward with the CF bond moving toward the CC bond. The HCH bond angle is greater than the tetrahedral angle in accord with decreased p character in the CH bond orbitals in response to the increased p character in the CF bond. The deviation of the two types of torsional angles from 60° is largely explained by the tilting of the CFH_2 groups. In contrast to the gauche rotamer, the projected angles for the CFH_2 group are 118.3° for the FCH angle and 123.4° for the HCH angles. Because of symmetry constraints FF repulsion cannot be relieved by rotation around the CC bond.

The somewhat longer CC bond in the anti rotamer of DFEA is consistent with Wiberg's analysis that attributes the gauche effect, the relatively lower energy of the gauche rotamer, to a *de*stabilization of the anti rotamer.[17] That the CC bond is not even shorter in the gauche rotamer can be attributed to the effect of FF repulsion in this rotamer. To counter the contribution of evident FF repulsion in the gauche rotamer, the destabilization in the anti rotamer must be significant.

Figure 11 gives the torsional angles for the two rotamers of TFEA. Other structural parameters for these two rotamers are in Table 5. The F_aCH and F_gCH angles for the gauche rotamer of TFEA are 108.8° and 107.7°, respectively. These angles were omitted from the microwave paper.[1] The obvious consequence of FF repulsion in the gauche rotamer is the value of 67.3° for the two F_aCCF_g torsional angles. The CF_2H groups rotate away from each other in the HCCH sense around the CC bond. Thus, the F_aCCF_a torsional angle is decreased to 51.9°, the two $HCCF_g$ angles are decreased to 54.2°, and the HCCH torsional angle is increased to 65.2°. The repulsion between the two CF_a bonds that are squeezed together by the internal rotation is relieved by the increase in the CCF_a bond angles to 110.1°. Because of the increased p character in the CF bond orbitals, these angles should have been less than the tetrahedral angle. The CCF_g and the FCF angles are indeed somewhat less than the tetrahedral angle. Also, the CCH angle of 112.4° is greater than the tetrahedral angle even though the F_aCH and F_gCH angles of 108.8° and 107.7°, respectively, seem too small.

As in the gauche rotamer of DFEA, the interpretation of relief of FF repulsion in gauche TFEA by group rotation around the CC bond is supported by considering projected angles. For the projection of the two HCF angles and the one FCF angle on a plane perpendicular to the CC bond, the results are 119.4°, 121.5°, and 119.2°, respectively, each close to 120°.

In the anti rotamer of TFEA, FF repulsion cannot be relieved by relatively unopposed rotation around the CC bond. Instead, relief comes from relatively small, energy-costly adjustments in bond angles. For the anti rotamer of TFEA, the FCCF angle of 63.6° reflects FF repulsion at the expense of the weaker HF repulsion. The CCF angle of 108.5° is consistent with increased p character in the CF bond orbitals, notwithstanding competing FF repulsion. The small FCF angle of 107.4° is also consistent with the enhanced p character of the CF bond orbitals. The large CCH angle of 112.9° conforms to the decreased CCF angle. The CF bond length in the anti rotamer correlates with the longer CF_g bonds in the gauche rotamer. This same correlation was found in the calculations. Possibly, this pattern reflects a trans−trans CF bond interaction. For the anti rotamer of TFEA the projected angles of the CF_2H groups are 116.4° and 121.8° for the HCF and FCF angles, respectively. As expected, these angles are more different from 120° than for the gauche rotamer that relaxes by internal rotation around the CC bond.

Another way to see the FF replusion is to consider the nonbonded distance between vicinal fluorine atoms. In the gauche rotamer of DFEA, which relieves FF repulsion by rotation around the CC bond, we find the largest FF distance of 2.897 Å, which corresponds to the largest FCCF torsion angle of 71.3°. In the gauche rotamer of TFEA, the F_gF_a distance is a smaller value of 2.797 Å, which corresponds to the smaller FCCF torsion angle of 67.3°. Relief of FF repulsion by internal rotation of the CF_2H groups in gauche TFEA is inhibited by F_aF_a repulsion, which gives the smallest of the vicinal FF distances, 2.673 Å. For the anti rotamer of TFEA, for which internal rotation of the CF_2H groups cannot relieve FF repulsion, the FF distance has the intermediate value of 2.734 Å.

Regarding the absence of an obvious gauche effect between the two rotamers of TFEA, in that the anti rotamer has the lower energy, it is likely that the substantial FF repulsion in the gauche rotamer overwhelms any destabilization of the anti rotamer by the Wiberg mechanism.

Summary

Rotational structures in the two bands due to CF stretching in the high-resolution infrared spectra of the anti rotamer of TFEA and its d_2 and $^{13}C_2$ isotopomers have been recorded and analyzed. One band is of A/C-type; the other is of B-type. These gas-phase spectra were simplified by being recorded at −100 °C in a 3 m cell. Although not intended for use with highly asymmetric tops, LW software proved very useful in analyzing oblate-type as well as prolate-type series. Ground-state rotational constants for a Watson-type Hamiltonian have been been fitted for each of the isotopomers. A complete structure for the nonpolar anti rotamer of TFEA has been found from these rotational constants. A structure for the polar gauche rotamer is available from a recent microwave study. Calculated structures of the anti and gauche rotamers compare favorably with the observed structures. Differences in structural parameters for the two rotamers of TFEA and DFEA are analyzed qualitatively and found to be understandable in terms of a significant FF repulsion.

Acknowledgment. We are grateful to Jessica I. Chuang and Christiana C. Nwofor for their work in synthesizing the isotopomers of TFEA. We are also grateful to Christopher F. Neese who wrote the Visual Basic add-in to Microsoft Excel, assisted with other computer applications, and did some of the data analysis. Walter J. Lafferty provided welcome encouragement to pursue oblate-type series in the spectra of highly asymmetric tops. Stephen C. Stone's Ph.D. thesis at Cornell University was of considerable help in initiating this project. National Science Foundation grant CHE 9710375 supported much of this work; Oberlin College and Justus-Liebig-Universität supported the rest.

Supporting Information Available: Tables 1S−9S contain GSCDs and spectral lines with assoicated quantum numbers for the isotopomers. These tables also contain the statistics of fitting rotational constants to Hamiltonians. This material is available free of charge via the Internet at http://pubs.acs.org.

References and Notes

(1) Maté, B.; Hight Walker, A; Suenram, R. D.; Craig, N. C. *J. Phys. Chem. A* **2000**, *104*, 9489.

(2) Kalasinsky, V. F.; Anjaria, H. V.; Little, T. S. *J. Phys. Chem.* **1982**, *86*, 1351.

(3) Muir, M.; Baker, J. *Mol. Phys.* **1996**, *89*, 211.

(4) Papasavva, S.; Illinger, K. H.; Kenny, J. E. *J. Phys. Chem.* **1996**, *100*, 10100.

(5) Craig, N. C.; Chen, A.; Suh, K. H.; Klee, S.; Mellau, G. C.; Winnewisser, B. P.; Winnewisser, M. *J. Phys. Chem. A* **1997**, *101*, 9302.

(6) Stone, S. C.; Philips, L. A.; Fraser, G. T.; Lovas, F. J.; Xu, L.-H. *J. Mol. Spectrosc.* **1998**, *192*, 75.

(7) Brown, D. D.; Beagley, B. *J. Mol. Struct.* **1977**, *38*, 167.

(8) Henne, A. L.; Renoll, M. W. *J. Am. Chem. Soc.* **1936**, *58*, 887.

(9) Craig, N. C.; Chuang, J. I.; Nwofor, C. C.; Oertel, C. M. *J. Phys. Chem. A* **2000**, *104*, 10092.

(10) Smith, K.; Newnham, D.; Page, M.; Ballard, J.; Duxbury, G. *J. Quant. Spectrosc. Radiat. Transfer* **1998**, *59*, 437.

(11) Fayt, A.; Lahaye, J. G.; Lemaire, J.; Herlemont, F.; Bantegnie, J. G. *J. Mol. Spectrosc.* **1990**, *140*, 252.

(12) Winnewisser, B. P.; Reinstädler, J.; Yamada, K. M. T.; Behrend, J. *J. Mol. Spectrosc.* **1989**, *136*, 12.

(13) In ref 9, the standard numerical order for the normal modes of the d_2 species was not followed in order to make the correlation with the other two isotopic species simpler.

(14) In computing GSCDs, Stone et al.[6] used all possible difference combinations in which the upper states were common. As a consequence of this procedure, a number of observed lines were used more than once. Whereas they report 398 GSCDs formed from 522 lines, only 229 GSCDs were nonredundant.

(15) Gordy, W.; Cook, R. L. *Microwave Molecular Spectra*, *Techniques of Chemistry*, 3rd ed.; John Wiley and Sons: New York, 1984; Vol. XVIII, pp 661, 666.

(16) Takeo, H.; Matsumura, C.; Morino, Y. *J. Chem. Phys.* **1986**, *84*, 4205.

(17) Wiberg, K. B. *Acc. Chem. Res.* **1996**, *29*, 229.

(18) Smart, B. E. Fluorinated Organic Molecules. *Molecular Structure and Energetics*; VCH Publishers: New York, 1986; Vol. 3, Chapter 4, p 144.

(19) Based on Takeo et al.[16] and their definitions of hydrogen atom relationships in the gauche rotamer. They used the "t" designation where we have used "a". In Å. C: $x = \pm 0.668\ 00$; $y = \pm 0.582\ 12$; $z = \pm 0.330\ 86$. H_g: $x = \pm 0.514\ 16$; $y = \pm 0.485\ 45$; $z = \pm 1.415\ 51$. H_a: $x = \pm 1.211\ 12$; $y = \pm 1.509\ 24$; $z = \pm 0.132\ 00$. $\tau_{FCCH_g} = 49.0°$, $\tau_{H_gCCH_a} = 71.0°$, $\tau_{H_aCCH_a} = 48.7°$.

(20) The F···F nonbonded distance of 2.897 Å was computed from the geometric parameters reported in ref 16.

(21) Torsional parameters for the anti rotamer derived from ref 5. $\tau_{FCCH_g} = 61.7°$, $\tau_{H_gCCH_g} = 56.6°$.